

Clinically Aware Synthetic Image Generation for Concept Coverage in Chest X-ray Models

Amy Rafferty¹, Rishi Ramaesh², and Ajitha Rajan¹

¹ School of Informatics, University of Edinburgh, UK

² NHS Lothian, UK

Abstract. The clinical deployment of AI diagnostic models demands more than benchmark accuracy — it demands robustness across the full spectrum of disease presentations. However, publicly available chest radiographic datasets systematically underrepresent critical clinical feature combinations, leaving models under-trained precisely where clinical stakes are highest. We present CARS, a clinically aware and anatomically grounded framework that addresses this gap through principled synthetic image generation. CARS applies targeted perturbations to clinical feature vectors, enabling controlled insertion and deletion of pathological findings while explicitly preserving anatomical structure.

We evaluate CARS across seven backbone architectures by fine-tuning models on synthetic subsets and testing on a held-out MIMIC-CXR benchmark. Compared to prior feature perturbation approaches, fine-tuning on CARS-generated images consistently improves precision-recall performance, reduces predictive uncertainty, and improves model calibration. Structural and semantic analyses demonstrate high anatomical fidelity, strong feature alignment, and low semantic uncertainty. Independent evaluation by two expert radiologists further confirms realism and clinical agreement. As the field moves toward regulated clinical AI, CARS demonstrates that anatomically faithful synthetic data generation for better feature space coverage is a viable and effective strategy for improving both the performance and trustworthiness of chest X-ray classification systems — without compromising clinical integrity.

Keywords: Synthetic Medical Image Generation · Uncertainty Quantification · Clinical Concept Modelling.

1 Introduction

Deep learning models for chest X-ray interpretation achieve strong benchmark performance, driven by large-scale datasets such as MIMIC-CXR [8, 15, 16] and CheXpert [13, 4]. However, benchmark performance alone does not guarantee clinical reliability, owing to incomplete coverage of clinically meaningful patterns [27, 31, 28, 20]. A critical gap persists: available training datasets, despite their scale, systematically underrepresent the radiographically difficult concept combinations encountered by clinicians — rare co-occurring findings, subtle presentations, and diagnostically ambiguous configurations. We draw an important

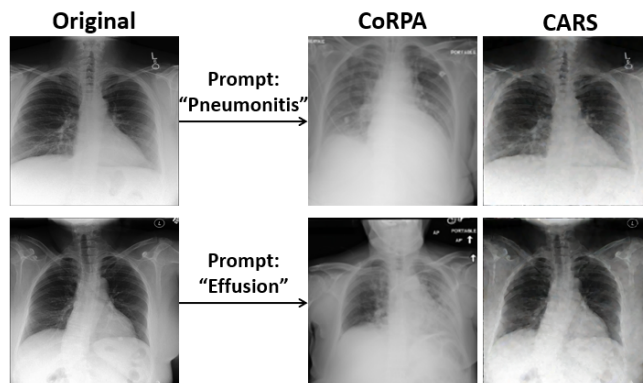


Fig. 1: Example synthetic images generated by CoRPA [25] and CARS (Ours). Image generation prompts for each approach were (1) Pneumonitis, (2) Effusion

distinction here between pathologies (diagnostic labels) and clinical concepts (the underlying radiographic features or findings that support them). Label diversity may appear high in existing datasets, but coverage of clinically meaningful concept combinations remains fundamentally limited, leaving models underprepared for real-world deployment where these gaps matter most.

Standard data augmentation strategies (rotation, flipping, intensity perturbation) improve robustness within the existing data distribution [11, 20, 27, 28] but cannot introduce genuinely novel clinical semantics. Synthetic chest radiography synthesis [30] offers a more powerful alternative, with GAN [9] and diffusion-based [32] approaches reporting gains in low-data and class-imbalanced settings [6, 3, 17]. However, most generative methods optimise for image-level realism without explicit control over clinical findings, increasing visual diversity without reliably expanding clinically meaningful concept coverage. To address this limitation, recent work, CoRPA, has explored *concept-driven* synthetic image generation, where structured clinical representations derived from radiology reports or expert-defined vocabularies are used to guide synthesis [25]. However, because synthesis is driven solely by perturbed reports, anatomical correspondence between source and synthetic chest radiographs is not preserved (Figure 1), introducing substantial structural inconsistencies (e.g., distorted lung fields or skeletal anatomy) that limit their practical utility.

We introduce **CARS** (Clinically Aware Radiograph Synthesis), an anatomically grounded refinement of concept-based chest X-ray synthesis. CARS preserves patient-specific anatomy by applying targeted perturbations in clinical concept space through image editing operations rather than full image generation. This design enables controlled modification of pathological findings while maintaining global radiographic structure, decoupling semantic expansion from uncontrolled anatomical variation.

We evaluate CARS across seven convolutional backbones using fine-tuning on synthetic data and testing on a held-out MIMIC-CXR benchmark. Beyond

classification performance (AUROC, AUPRC, F1), we assess model reliability through predictive uncertainty [2, 18] and calibration [7, 14], using entropy [10] and Expected Calibration Error (ECE) [24]. In medical imaging, failures often arise from semantically incorrect or incomplete findings rather than low-confidence predictions. We evaluate semantic concept alignment using a vision-language model [33] and a concept-level uncertainty framework [5] that compares inferred and ground-truth concept sets using set-based metrics (e.g., precision and recall), decomposing uncertainty into over- and under-prediction [19, 29]. We further assess the structural fidelity of synthetic images and conduct expert radiologist evaluation of image realism and clinical concordance. Across all evaluations, CARS consistently outperforms existing work [25], with improved precision–recall performance, reduced predictive and semantic uncertainty, and higher anatomical and clinical fidelity.

2 Materials and Experimental Setup

Dataset. We use the MIMIC-CXR dataset [15, 16, 8], a large public collection of chest radiographs paired with free-text radiology reports. We restrict the dataset to posteroanterior (PA) views to reduce variability in imaging geometry and interpretation. We do not use the provided dataset labels, which have been shown to be noisy and unreliable [21]. Instead, we re-annotate all images using an expert-defined clinical concept space, following existing work [25]. Under radiologist guidance, we focus on six clinically relevant diagnostic labels: **Pneumothorax** (features concerning for pleural air), **Pneumonia** (airspace disease consistent with infection), **Pleural Effusion** (pleural fluid or effusion-related findings), **Cardiomegaly** (enlarged cardiac silhouette), **Suspicious Malignancy** (features warranting lung cancer workup), and **No Relevant Finding** (absence of relevant abnormalities). The resulting dataset is highly imbalanced, with a predominance of normal studies; we undersample the **No Relevant Finding** class to twice the size of the largest abnormal class. The final dataset contains 40,083 images with multi-label annotations. We perform a multi-label stratified split into training (80%), validation (10%), and test (10%) sets. The held-out test set contains 4,008 images and is used for all experiments.

Clinical Concept Annotation. Each image is annotated by converting its associated radiology report into a binary clinical concept vector, using the CoRPA vocabulary [25]. Radiology reports are converted into binary vectors indicating the presence or absence of these predefined clinical concepts using expert-defined phrase mappings. Images may contain multiple concepts; when any pathology is present, the *Unremarkable* concept is suppressed. Clinical concepts are deterministically mapped to diagnostic labels, ensuring consistent annotation across real and synthetic data and enabling direct comparison in concept space. Our concept vocabulary, phrase mappings, and label definitions are publicly available.

Model Architectures. We train and evaluate seven convolutional backbones, matching CoRPA and the MICCAI CXR-LT challenge [12]: ConvNeXt-Base,

ConvNeXt-Small, DenseNet-161, EfficientNet-V2-S, ResNet-50, ResNet-101, and ResNeXt-101. All models are ImageNet-initialized and adapted for multi-label classification. Models are trained on MIMIC-CXR using a multi-label formulation, as images may contain co-occurring findings. Labels are encoded as multi-hot vectors, with **No Relevant Finding** treated implicitly as the absence of pathology labels. Images are converted to RGB and ImageNet-normalized. Training uses AdamW optimization with cosine scheduling and warm-up under mixed-precision CUDA training. We use binary cross-entropy with logits, and per-class positive weighting to address imbalance. Models are trained for 30 epochs (batch size 32, learning rate 3×10^{-4}). Performance is reported using macro-averaged AUROC, AUPRC, and F1, with per-class thresholds tuned on the validation set. To assess the impact of synthetic concept perturbations, each model is also fine-tuned on stratified subsets of synthetic images generated by CoRPA versus CARS. To ensure comparability, we uniformly sample 10,000 images from each method. Synthetic data are annotated using the same concept-to-label mapping as real data. Each subset is split into training/validation (80/20), and models are fine-tuned for five epochs using head-only adaptation. Final evaluation is performed on the original held-out MIMIC-CXR test set.

Experiments. We evaluate baseline models and models fine-tuned on CoRPA versus CARS synthetic data using macro-averaged AUROC, AUPRC, and F1 on a held-out MIMIC-CXR test set. Predictive reliability is assessed using predictive entropy and Expected Calibration Error (ECE), computed from model output probabilities. These metrics capture both classification performance and confidence calibration across architectures. We also assess the quality of synthetic images in terms of anatomical fidelity and semantic concept alignment. Anatomical fidelity is measured using the Structural Similarity Index (SSIM) between original and synthetic image pairs (mean \pm standard deviation). Semantic alignment is evaluated using a concept-level pipeline adapted from [5]: synthetic images are processed with LLaVA-Rad [33] to generate descriptions, which are mapped to clinical feature vectors and compared to ground-truth perturbed concepts using Jaccard similarity and normalized Hamming distance. Semantic uncertainty is also quantified via $U_{FP} = 1 - \text{Precision}$ (hallucinated findings) and $U_{FN} = 1 - \text{Recall}$ (missed findings). Finally, two independent radiologists evaluated 50 CoRPA and 100 CARS synthetic images. Images are assessed for perceived realism (real vs. synthetic) and agreement with proposed clinical concepts (full, partial, or disagree). Free-text justifications are collected for images judged synthetic or with concept disagreement. We report response distributions and inter-rater agreement as qualitative validation of clinical plausibility.

3 CARS Framework

CARS expands clinically meaningful concept coverage in chest X-ray data while preserving the anatomical correspondence to real radiographs, by applying structured perturbations in clinical concept space and translating them into local-

ized image edits on an original scan. CARS has three stages. First, each image-report pair is encoded as a binary clinical concept vector indicating the presence of expert-defined radiological findings. Second, the concept vector is modified using clinically motivated perturbations—*Intra-Class*, *Insertion*, and *Deletion*—to introduce plausible but under-represented concept combinations. Third, the perturbed vector is converted to a concise clinical prompt and passed to RadEdit [22], which applies spatially localized edits to express the intended changes while preserving global anatomy. By operating at the concept level while enforcing anatomical grounding, CARS decouples semantic expansion from uncontrolled structural variation, enabling exploration of clinically relevant concept combinations with preserved radiographic plausibility.

Concept Perturbation Strategies. Each image is represented by a binary clinical concept vector, with an associated diagnostic label set induced by the concept-to-label mapping (Section 2). CARS generates perturbed concept vectors using three clinically motivated strategies. **Intra-Class** modifies concepts associated with the ground-truth label to represent alternative but valid manifestations of the same condition, capturing within-diagnosis variability. **Insertion** adds concepts from an additional pathology label while retaining the original label set, simulating multi-pathology presentations or spurious findings. **Deletion** removes concepts associated with a selected pathology. In multi-label cases, one label is randomly removed; in single-label abnormal cases, concepts are replaced with *Unremarkable*, simulating a missed diagnosis. Intra-class perturbations are undefined for single-concept pathologies (e.g., **Cardiomegaly**). For deletion, single-label abnormal cases are mapped to **No Relevant Finding**. Up to two unique perturbations per type are otherwise generated for each image.

Anatomy-Preserving Image Editing. Each perturbed concept vector is converted into a concise clinical prompt listing the target findings. We do not explicitly specify removals; instead, RadEdit is conditioned on the target findings to exist in the edited image. Given an original radiograph x , RadEdit generates an edited image x' that expresses the intended diagnostic changes while preserving anatomical correspondence. RadEdit applies fine-grained, spatially localized edits using a latent diffusion model [26] with a BioViL-T text encoder [1] and an SDXL-VAE autoencoder [23]. Unlike full-image synthesis, RadEdit edits the source radiograph directly, promoting preservation of global structure (e.g., lung fields and skeletal anatomy) while enabling localized pathological changes. Trained on MIMIC-CXR with report-style supervision aligned to our annotation pipeline, RadEdit interprets our concept-derived prompts with high fidelity, producing anatomically consistent and radiologically coherent outputs.

4 Results

Model Performance and Uncertainty. Table 1 reports multi-label classification performance across seven backbones. Baseline models trained on MIMIC-

Table 1: Macro-averaged AUROC, AUPRC, and F1 across seven backbones. We report baseline performance and differences (\uparrow / \downarrow) after fine-tuning on synthetic 1. CARS (Ours) images, 2. CoRPA images, evaluated on a held-out test set ($N = 4008$). F1 thresholds are calibrated on the validation set; improvements are in **bold**.

| | | Con-B | Con-S | Dense | Effic | Res50 | Res101 | ResNXt |
|------------------------|----------------|-------------------------|-------------------------|-------------------------|-------------------------|-------------------------|-------------------------|-------------------------|
| Baseline | AUROC | 0.947 | 0.940 | 0.922 | 0.943 | 0.913 | 0.926 | 0.949 |
| | AUPRC | 0.864 | 0.838 | 0.772 | 0.839 | 0.719 | 0.786 | 0.869 |
| | F1 | 0.835 | 0.802 | 0.734 | 0.797 | 0.677 | 0.740 | 0.844 |
| Finetuned CARS | Δ AUROC | \downarrow 0.007 | \downarrow 0.008 | \downarrow 0.008 | \downarrow 0.010 | \uparrow 0.003 | \downarrow 0.007 | \downarrow 0.009 |
| | Δ AUPRC | \uparrow 0.048 | \uparrow 0.052 | \uparrow 0.110 | \uparrow 0.026 | \uparrow 0.087 | \uparrow 0.058 | \downarrow 0.003 |
| | Δ F1 | \uparrow 0.087 | \uparrow 0.092 | \uparrow 0.096 | \uparrow 0.019 | \uparrow 0.102 | \uparrow 0.033 | \uparrow 0.002 |
| Finetuned CoRPA | Δ AUROC | \downarrow 0.015 | \downarrow 0.016 | \downarrow 0.014 | \downarrow 0.012 | \downarrow 0.021 | \downarrow 0.019 | \downarrow 0.008 |
| | Δ AUPRC | \downarrow 0.061 | \downarrow 0.058 | \downarrow 0.074 | \downarrow 0.055 | \downarrow 0.077 | \downarrow 0.082 | \downarrow 0.036 |
| | Δ F1 | \downarrow 0.137 | \downarrow 0.131 | \downarrow 0.136 | \downarrow 0.077 | \downarrow 0.129 | \downarrow 0.155 | \downarrow 0.102 |

Table 2: Predictive entropy and Expected Calibration Error (ECE) across seven backbones. We report baseline performance and differences (\uparrow / \downarrow) after fine-tuning on synthetic 1. CARS (Ours) images, 2. CoRPA images, evaluated on a held-out test set ($N = 4008$) and macro-averaged across labels. Reductions are shown in **bold**.

| | | Con-B | Con-S | Dense | Effic | Res50 | Res101 | ResNXt |
|------------------------|------------------|---------------------------|---------------------------|---------------------------|---------------------------|---------------------------|---------------------------|---------------------------|
| Baseline | Entropy | 0.086 | 0.135 | 0.225 | 0.123 | 0.265 | 0.201 | 0.043 |
| | ECE | 0.045 | 0.063 | 0.093 | 0.062 | 0.114 | 0.085 | 0.040 |
| Finetuned CARS | Δ Entropy | \downarrow 0.012 | \downarrow 0.022 | \uparrow 0.026 | \uparrow 0.024 | \downarrow 0.105 | \downarrow 0.075 | \downarrow 0.002 |
| | Δ ECE | \downarrow 0.012 | \downarrow 0.008 | \downarrow 0.014 | \downarrow 0.010 | \downarrow 0.031 | \uparrow 0.006 | \downarrow 0.009 |
| Finetuned CoRPA | Δ Entropy | \uparrow 0.057 | \uparrow 0.055 | \uparrow 0.062 | \uparrow 0.071 | \uparrow 0.032 | \uparrow 0.035 | \uparrow 0.062 |
| | Δ ECE | \uparrow 0.094 | \uparrow 0.097 | \uparrow 0.080 | \uparrow 0.125 | \uparrow 0.051 | \uparrow 0.083 | \uparrow 0.154 |

CXR achieve strong macro-AUROC and AUPRC. Fine-tuning with CARS synthetic images consistently improves macro-AUPRC and macro-F1 across all architectures, with the largest gains observed for DenseNet-161, ResNet-50, and ConvNeXt. Although AUROC changes are modest and occasionally negative, systematic improvements in AUPRC and F1 indicate better precision–recall trade-offs under class imbalance. In contrast, CoRPA fine-tuning degrades performance across metrics, suggesting that unconstrained concept perturbations introduce noise that impairs learning. Table 2 summarizes predictive entropy and Expected Calibration Error (ECE) after fine-tuning. CARS reduces entropy for most architectures—particularly ResNet-50, ResNet-101, and ConvNeXt—and improves calibration, with ECE decreasing for six of seven models. CoRPA instead consistently increases both entropy and ECE, reflecting higher uncertainty and degraded calibration. These results indicate that CARS improves predictive reliability as well as classification performance, underscoring the importance of anatomically and semantically grounded synthetic augmentation.

Table 3: Structural Similarity (SSIM) between original and synthetic chest X-rays for CARS (Ours) and CoRPA.

| Perturbation Type | CARS | CoRPA |
|-------------------|-------------------------------------|-------------------------------------|
| Intra-class | 0.748 ± 0.030 | 0.304 ± 0.063 |
| Insertion | 0.751 ± 0.032 | — |
| Deletion | 0.749 ± 0.030 | — |
| Outer-class | — | 0.229 ± 0.102 |
| Overall | 0.750 ± 0.031 | 0.273 ± 0.089 |

Table 4: Semantic concept uncertainty for CARS (Ours) and CoRPA synthetic images, reported as mean \pm standard deviation ($N = 10,000$).

| | Jaccard | Hamming | $U_{FP} = 1 - \text{Prec}$ | $U_{FN} = 1 - \text{Rec}$ |
|--------------|-------------------|-------------------|----------------------------|---------------------------|
| CARS | 0.609 ± 0.149 | 0.092 ± 0.043 | 0.489 ± 0.211 | 0.287 ± 0.114 |
| CoRPA | 0.168 ± 0.327 | 0.113 ± 0.068 | 0.799 ± 0.359 | 0.595 ± 0.488 |

Structural Fidelity and Semantic Uncertainty. Anatomical consistency is evaluated using the Structural Similarity Index (SSIM), reported in Table 3. CARS-generated images achieve substantially higher SSIM than CoRPA across all perturbation types, with an overall mean of 0.750 ± 0.031 versus 0.273 ± 0.089 , indicating markedly better preservation of anatomical structure. Within CARS, intra-class, insertion, and deletion perturbations yield comparable SSIM values, demonstrating that targeted concept edits can be applied without disrupting global anatomy. In contrast, CoRPA—particularly outer-class perturbations—exhibits very low SSIM, reflecting large structural divergence from source images. These results confirm that CARS expands the clinical concept space while maintaining anatomical correspondence (Figure 1). Table 4 reports semantic agreement between ground-truth concept vectors and those inferred by LLaVA-Rad. CoRPA exhibits low semantic overlap (Jaccard 0.168 ± 0.327) and high Hamming distance (0.113 ± 0.068), with high over- and under-prediction uncertainty ($U_{FP} = 0.799 \pm 0.359$, $U_{FN} = 0.595 \pm 0.488$), indicating frequent hallucinated and missed findings. CARS demonstrates improved concept alignment, with higher Jaccard similarity (0.609 ± 0.149), lower Hamming distance (0.092 ± 0.043), and reduced over- and under-prediction uncertainty ($U_{FP} = 0.489 \pm 0.211$, $U_{FN} = 0.287 \pm 0.114$). Lower variance across images further suggests more consistent semantic grounding. Together, these results indicate that CARS more reliably conveys intended clinical concepts.

Expert Evaluation. Expert evaluation results (Section 2) are summarized in Table 5. Both radiologists judged CARS images as real more frequently than CoRPA images (R1: 94% vs. 86%; R2: 88% vs. 62%) and reported higher full agreement with the targeted clinical concepts. Inter-rater agreement was moderate, with agreement on realism for 61% of images and on clinical concept judgments for 72%. Free-text analysis highlights qualitative differences in failure

Table 5: Expert evaluation of CARS ($N = 100$) and CoRPA ($N = 50$) synthetic chest X-rays by two independent radiologists (Expert 1, Expert 2).

| Task | Assessment | CARS | | CoRPA | |
|--------------------|---------------|------------|------------|------------|------------|
| | | Expert 1 | Expert 2 | Expert 1 | Expert 2 |
| Real/Synthetic | Real | 94% | 88% | 86% | 62% |
| | Synthetic | 6% | 12% | 14% | 38% |
| Clinical Agreement | Fully Agree | 61% | 59% | 46% | 52% |
| | Partial Agree | 22% | 21% | 24% | 24% |
| | Disagree | 17% | 20% | 30% | 24% |

modes. CoRPA images judged synthetic were primarily attributed to anatomical inconsistencies, including implausible rib spacing, clavicular asymmetry, distorted cardiac contours, and non-physiological lung textures. Concept disagreements frequently involved over-specified or weakly supported findings and missing hallmark signs. In contrast, CARS images rarely exhibited major anatomical errors; images judged synthetic were described as “too clean” or showed subtle textural artifacts. Concept disagreements in CARS cases mainly reflected secondary or borderline findings, often characterized by inherent diagnostic ambiguity (e.g., “subtle” or “not definitive”). Overall, CARS reduces major anatomical and semantic failures and shifts uncertainty toward clinically realistic ambiguity. While CoRPA errors commonly stem from structural implausibility or concept hallucination, CARS’s uncertainty more closely resembles that encountered in real-world radiographic interpretation, supporting the value of anatomical grounding in synthetic chest X-ray generation.

5 Conclusion

We presented CARS, a clinically aware and anatomically grounded framework for concept-based synthetic chest X-ray generation. By translating structured concept perturbations into anatomy-preserving image edits, CARS expands clinically meaningful concept coverage while maintaining radiographic plausibility. Across seven backbone architectures, fine-tuning with CARS consistently improved multi-label performance, reduced predictive uncertainty, and improved calibration. CARS-generated images demonstrate high structural fidelity and strong semantic alignment between intended and inferred clinical concepts. Compared to existing work, CARS substantially reduces both over- and under-prediction at the concept level and shifts failure modes toward clinically realistic ambiguity. Radiologist evaluation further supports improved realism and clinical agreement. These results show that anatomically grounded concept perturbations enhance the effectiveness and reliability of synthetic data for chest X-ray modelling. Future work will extend CARS to broader concept spaces, additional modalities, and alternative semantic uncertainty frameworks.

Code and concepts: <https://anonymous.4open.science/r/CARS-3BAF/>.

References

1. Bannur, S., Hyland, S., Liu, Q., Perez-Garcia, F., Ilse, M., Castro, D.C., Boecking, B., Sharma, H., Bouzid, K., Thieme, A., et al.: Learning to exploit temporal structure for biomedical vision-language processing. In: Proceedings of the IEEE/CVF Conference on Computer Vision and Pattern Recognition. pp. 15016–15027 (2023)
2. Begoli, E., Bhattacharya, T., Kusnezov, D.: The need for uncertainty quantification in machine-assisted medical decision making. *Nature Machine Intelligence* **1** (2019)
3. Chaichuk, M., Gautam, S., Hicks, S., Tutubalina, E.: Prompt to polyp: Medical text-conditioned image synthesis with diffusion models (2025)
4. Chambon, P., Delbrouck, J.B., Sounack, T., Huang, S.C., Chen, Z., Varma, M., Truong, S.Q., Chuong, C.T., Langlotz, C.P.: Chexpert plus: Augmenting a large chest x-ray dataset with text radiology reports, patient demographics and additional image formats. *arXiv:2405.19538* (2024)
5. Franchi, G., Trong, D.N., Belkhir, N., Xia, G., Pilzer, A.: Towards understanding and quantifying uncertainty for text-to-image generation (2024)
6. Frid-Adar, M., Diamant, I., Klang, E., Amitai, M., Goldberger, J., Greenspan, H.: Gan-based synthetic medical image augmentation for increased cnn performance in liver lesion classification. *Neurocomputing* **321**, 321–331 (Dec 2018)
7. Ghesu, F.C., Georgescu, B., Gibson, E., Guendel, S., Kalra, M.K., Singh, R., Digumarthy, S.R., Grbic, S., Comaniciu, D.: Quantifying and leveraging classification uncertainty for chest radiograph assessment (2019)
8. Goldberger, A.L., Amaral, L.A., Glass, L., Hausdorff, J.M., Ivanov, P.C., Mark, R.G., Mietus, J.E., Moody, G.B., Peng, C.K., Stanley, H.E.: Physiobank, physiotoolkit, and physionet: components of a new research resource for complex physiologic signals. *circulation* **101**(23), e215–e220 (2000)
9. Goodfellow, I., Pouget-Abadie, J., Mirza, M., Xu, B., Warde-Farley, D., Ozair, S., Courville, A., Yere, Y.: Generative adversarial networks. *Advances in Neural Information Processing Systems* **3** (06 2014)
10. Hernandez-Lobato, J.M., Hoffman, M.W., Ghahramani, Z.: Predictive entropy search for efficient global optimization of black-box functions. In: *Advances in Neural Information Processing Systems*. pp. 918–926. Curran Associates Inc. (2014)
11. Hinton, G., Krizhevsky, A., Sutskever, I., Rachmad, Y.: Imagenet classification with deep convolutional neural networks. *Advances in Neural Information Processing Systems* pp. 1097–1105 (01 2012)
12. Holste, G., Wang, S., Jaiswal, A., Yang, Y., Lin, M., Peng, Y., Wang, A.: Cxr-It: Multi-label long-tailed classification on chest x-rays. *PhysioNet* **5**(19), 1 (2023)
13. Irvin, J., Rajpurkar, P., Ko, M., Yu, Y., Ciurea-Ilcus, S., Chute, C., Marklund, H., Haghgoo, B., Ball, R., Shpanskaya, K., et al.: Chexpert: A large chest radiograph dataset with uncertainty labels and expert comparison. In: *Proceedings of the AAAI conference on artificial intelligence*. vol. 33, pp. 590–597 (2019)
14. Jiang, H., Kim, B., Guan, M.Y., Gupta, M.: To trust or not to trust a classifier (2018)
15. Johnson, A.E., Pollard, T.J., Berkowitz, S.J., Greenbaum, N.R., Lungren, M.P., Deng, C.y., Mark, R.G., Horng, S.: Mimic-cxr, a de-identified publicly available database of chest radiographs with free-text reports. *Scientific data* **6**(1) (2019)
16. Johnson, A.E., Pollard, T.J., Greenbaum, N.R., Lungren, M.P., Deng, C.y., Peng, Y., Lu, Z., Mark, R.G., Berkowitz, S.J., Horng, S.: Mimic-cxr-jpg, a large publicly available database of labeled chest radiographs. *arXiv:1901.07042* (2019)

17. Kazerouni, A., Aghdam, E.K., Heidari, M., Azad, R., Fayyaz, M., Hacihaliloglu, I., Merhof, D.: Diffusion models in medical imaging: A comprehensive survey. *Medical Image Analysis* **88**, 102846 (2023)
18. Kompa, B., Snoek, J., Beam, A.: Second opinion needed: communicating uncertainty in medical machine learning. *npj Digital Medicine* **4** (12 2021)
19. Kuhn, L., Gal, Y., Farquhar, S.: Semantic uncertainty: Linguistic invariances for uncertainty estimation in natural language generation (2023)
20. Litjens, G., Kooi, T., Bejnordi, B.E., Setio, A.A.A., Ciompi, F., Ghafoorian, M., van der Laak, J.A., van Ginneken, B., Sánchez, C.I.: A survey on deep learning in medical image analysis. *Medical Image Analysis* **42**, 60–88 (Dec 2017)
21. McDermott, M.B., Hsu, T.M.H., Weng, W.H., Ghassemi, M., Szolovits, P.: Chexpert++: Approximating the chexpert labeler for speed, differentiability, and probabilistic output. In: *ML for Healthcare Conference*. pp. 913–927. PMLR (2020)
22. Pérez-García, F., Bond-Taylor, S., Sanchez, P.P., van Breugel, B., Castro, D.C., Sharma, H., Salvatelli, V., Wetscherek, M.T., Richardson, H., Lungren, M.P., et al.: Radedit: stress-testing biomedical vision models via diffusion image editing. In: *European Conference on Computer Vision*. pp. 358–376. Springer (2024)
23. Podell, D., English, Z., Lacey, K., Blattmann, A., Dockhorn, T., Müller, J., Penna, J., Rombach, R.: Sdxl: Improving latent diffusion models for high-resolution image synthesis. arXiv:2307.01952 (2023)
24. Posocco, N., Bonnefoy, A.: Estimating expected calibration errors (2021)
25. Rafferty, A., Ramaesh, R., Rajan, A.: Corpa: Adversarial image generation for chest x-rays using concept vector perturbations and generative models (2025)
26. Rombach, R., Blattmann, A., Lorenz, D., Esser, P., Ommer, B.: High-resolution image synthesis with latent diffusion models. In: *Proceedings of the IEEE/CVF conference on computer vision and pattern recognition*. pp. 10684–10695 (2022)
27. Roth, H., Lu, L., Liu, J., Yao, J., Seff, A., Kim, L., Summers, R.: Improving computer-aided detection using convolutional neural networks and random view aggregation. *IEEE transactions on medical imaging* (09 2015)
28. Shi, J., Zhou, S., Liu, X., Zhang, Q., Lu, M., Wang, T.: Stacked deep polynomial network based representation learning for tumor classification with small ultrasound image dataset. *Neurocomput.* **194**(C), 87–94 (Jun 2016)
29. Singhal, K., Azizi, S., Tu, T., Mahdavi, S.S., Wei, J., Chung, H.W., Scales, N., Tanwani, A., Cole-Lewis, H., Pfohl, S., et al., P.P.: Large language models encode clinical knowledge (2022)
30. Sundaram, S., Hulkund, N.: Gan-based data augmentation for chest x-ray classification (2021)
31. Tajbakhsh, N., Shin, J., Gurudu, S., Hurst, R.T., Kendall, C., Gotway, M., Liang, J.: Convolutional neural networks for medical image analysis: Fine tuning or full training? *IEEE Transactions on Medical Imaging* **35**, 1–1 (03 2016)
32. Yang, L., Zhang, Z., Song, Y., Hong, S., Xu, R., Zhao, Y., Zhang, W., Cui, B., Yang, M.H.: Diffusion models: A comprehensive survey of methods and applications (2025)
33. Zambrano Chaves, J.M., Huang, S.C., Xu, Y., Xu, H., Usuyama, N., Zhang, S., Wang, F., Xie, Y., Khademi, M., Yang, Z.e.a.: A clinically accessible small multimodal radiology model and evaluation metric for chest x-ray findings. *Nature Communications* **16** (04 2025)